6 TIME OF FLIGHT MEASUREMENTS

In the framework of the HADES spectrometer a time of flight system has been adopted, in order to select efficiently rare events with dilepton pairs produced in nuclear and elementary collisions, in combination with RICH and Shower subdetectors.

Moreover the time of flight (tof) measure allows to perform even hadron identification, in combination with the momentum information given by the tracking system, and to separate protons from pions with good efficiency and purity [Tlu04]. Indeed hadron identification is mandatory to perform exclusive analysis on decay channels in elementary collisions, where the identification of all the outgoing charged particles is needed.

The time of flight system is constituted by three detectors which are START, placed along the beam, TOF and TOFINO placed after the magnetic field region, respectively at higher and lower polar angles.

The start signal is given by the 1st level trigger, which correlates the multiplicity information from META to the combined information from START and VETO detectors; the logical signal is sent to TDCs to start the tof measure, while the STOP is given by TOF and TOFINO detectors.

In order to provide a good timing resolution, a calibration procedure is foreseen and it will be presented in the next paragraphs, which involves time calibration for the three subdetectors and position calibration for the only TOF system; the resolution values obtained in proton experimental runs will be also shown.

In January 2004 the START detector was not used, so it was necessary to implement a new calibration procedure for the tof walls, and an algorithm to reconstruct the start time of the reactions. Resolution and efficiency values of the method will be shown and compared for simulation and experimental data.

6.1 Calibration parameters

6.1.1 START hodoscope

The time of flight (*tof*) value given by TDCs can be considered in general as the difference between arrival times of the stop signal t_{STOP} (given by TOF or TOFINO), and the start one t_{START} given by the 1st level trigger:

$$tof = t_{STOP} - t_{START} \qquad \textbf{(Eq. 6-1)}$$

The START detector for proton experiment (hodoscope) is constituted by 16 scintillator small rods (stripes); each one is connected to a photomultiplier and to its own electronic chain. This means the signals from each stripe reach 1st level trigger system with its own delay time, due to cable lengths and electronics.

If we assume a particle hit a START strip *i* after a time t_0, the signal reaches the trigger system after a time t^{i}_{START}, given by:

$$t^{i}_{START} = t_0 - t^{i}_{offset} \qquad \textbf{(Eq. 6-2)}$$

there t^{i}_{offset} is the time offset of each different stripe.

Each one of these offsets has to be calculated in order that the whole START system provides its signals with a timing which does not depend on the hit stripe. After the START calibration procedure, these offsets will be subtracted stripe-wise to the time given by META detectors.

6.1.2 TOF wall

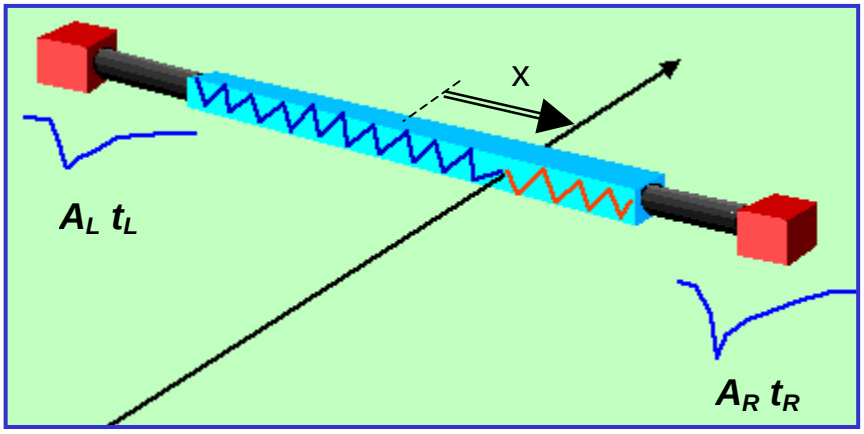

Figure 6.1 – Scheme of a TOF scintillator rod and of its coordinate system.

Figure 6.1 shows the scheme of a TOF rod hit by a particle. The particle generates a light signal proportional in intensity to the released energy, and this signal will reach the rod ends after a time t_R for the right end, t_L for the left one. We can express these two times by the equations:

$$t_R(x) = tof + \frac{1}{Vg}\left(\frac{L}{2} + x\right) + D_R \qquad \textbf{(Eq. 6-3)}$$

$$t_L(x) = tof + \frac{1}{Vg}\left(\frac{L}{2} - x\right) + D_L \qquad \textbf{(Eq. 6-4)}$$

where *tof* is the particle time of flight (assuming the START signal has been corrected), x is its distance from the rod centre, L and Vg are respectively the rod length and the group velocity of the light signal, $D_{L,R}$ are the offsets connected to discriminators, electronic chains and cable length for left and right channels.

From the previous equations we can calculate not only the particle *tof* , but even its hit position in the rod x:

$$tof = \frac{1}{2}(t_R + t_L) + t_{offset} \qquad \textbf{(Eq. 6-5)}$$

$$x = \frac{1}{2}(t_R - t_L)\cdot Vg + x_{offset} \qquad \textbf{(Eq. 6-6)}$$

where t_{offset} and x_{offset} are respectively time and position offsets, given by:

$$t_{offset} = -\frac{1}{2}\left(\frac{L}{Vg} + D_R + D_L\right) \qquad \textbf{(Eq. 6-7)}$$

$$x_{offset} = -\frac{Vg}{2}(D_R - D_L) \qquad \textbf{(Eq. 6-8)}$$

The group velocity is known from measures done by using a laser system, so TOF calibration consists on calculating for each rod the values of position and time offsets[1].

The amplitude information was not used in proton experiment; further information on ADC calibration can be found in [Spa02].

6.1.3 TOFINO wall

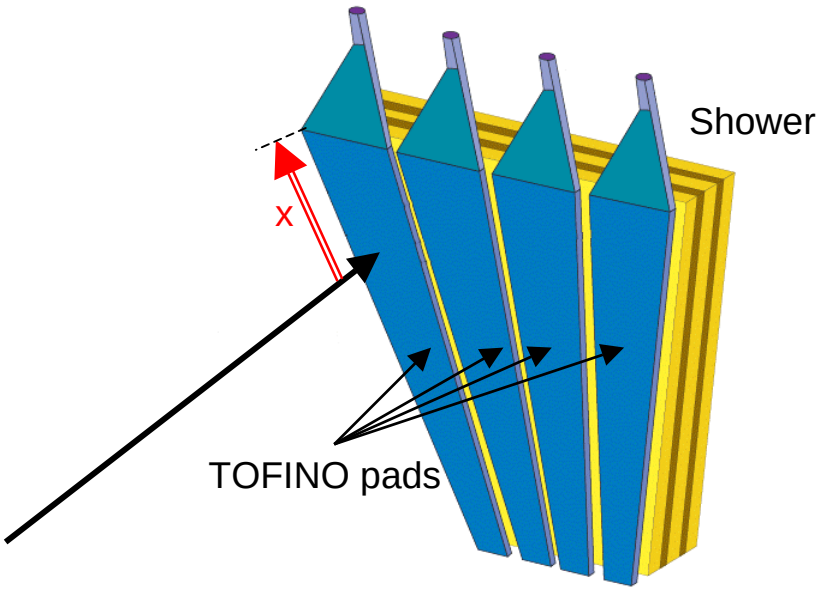

Figure 6.2 – Scheme of TOFINO detector. The position information is given by Shower pads.

---

[1] In effect the signal from TDCs is expressed in channel values t^c [0,4096]. In order to convert these values into nanoseconds they have to be recalculated as:

$$t_{L.R} = k_{L,R}t^c_{L,R} + O_{L,R}$$

where k are the nanosecond/channel slopes which depend on only TDCs, calculated on bench, while O are the time offsets that can be included inside the global offsets t_{offset} and x_{offset}.

The principle of TOFINO wall is similar to the TOF one, but in this case the light signal is collected only at one edge of the scintillator pad.

Figure 6.2 shows a scheme of the TOFINO principle; when a particle hits one pad it produces a light signal, which crosses the scintillator material and reaches the PMT edge after a time *t* given by:

$$t = tof + \frac{x}{Vg} + t_{offset} \qquad \textbf{(Eq. 6-9)}$$

where *x* is the hit distance from the PMT edge, *Vg* is the light group velocity in the scintillator and t_{offset} is the time offset.

Using only TOFINO it is not possible to have the position information of the hit, but we can obtain this information by correlation to Shower system, which is segmented into several pads and provides positions with a resolution given by the pad size (2-5 cm). So for TOFINO calibration only time offsets must be calculated.

6.2 TOF position calibration

The information of the particle hit in TOF rods it is important in both on-line and off-line analysis.

During data acquisition the 2nd level trigger correlates in position hits in RICH detector with TOF positions, in order to select events which contain candidate leptons; in order to assign the correct tof to reconstructed tracks TOF correlation is needed with the tracking system, and by knowing the exact point in space where the particle gives the signal in META detectors we can calculate the track path length. Moreover META hit position is used by kickplane algorithm (5.3.1) to reconstruct momenta for sectors without outer MDC chambers (so for November 2002 analysis).

The TOF position calibration is made through correlation to MDC segments, by analysing straight tracks in no field data[2]. The procedure is the following.

Let assume a particle emitted inside the target crosses MDC chambers and TOF wall, providing a useful signal in both the detectors. By projecting the segment reconstructed by drift chambers toward TOF system, we can calculate the position of the projected point, and its distance from the hit measured by the scintillator rod.

Figure 6.3 outlines the procedure. If we consider the plane that crosses the hit rod perpendicular to the beam direction, the position of the projected hit along the rod direction x_{MDC} will be given by:

$$x_{MDC} = \frac{Y_{TOF}}{\tan(\Phi_{MDC})} \qquad \textbf{(Eq. 6-10)}$$

where Φ_{MDC} is the azimuthal angle measured by MDC segment, while Y_{TOF} is the y position of the rod in the laboratory coordinate system, which is fixed by the detector geometry. The procedure can be used for both inner and outer drift chambers, and we expect to obtain the same results.

[2] Position calibration can be done even using field data by the same procedure, but in this case the ϕ bending from the magnetic field decreases the quality of the obtained position resolution.

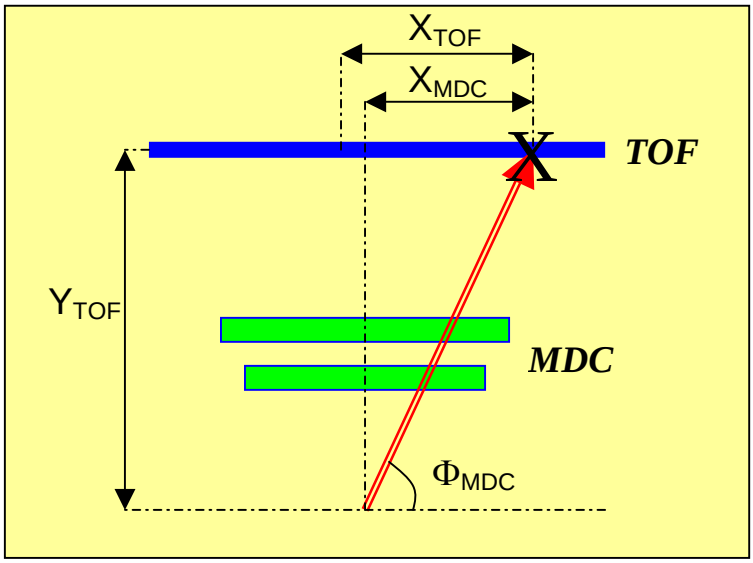

Figure 6.3 – Scheme of TOF position calibration procedure by using MDC correlation.

We can consider the position errors for the projected hit almost negligible, because of MDC resolution (below 1 mm) which is much lower respect to the TOF one (few centimetres). From the width of residuals after calibration we can evaluate even TOF position resolution.

For the position calibration only inner segments were used, and after the results were compared to what obtained using outer chambers.

In Figure 6.4 the residuals for January 2004 data are plotted in function of TOF rod number (one sector is made by 64 rods), for inner and outer chambers, after the position calibration procedure.

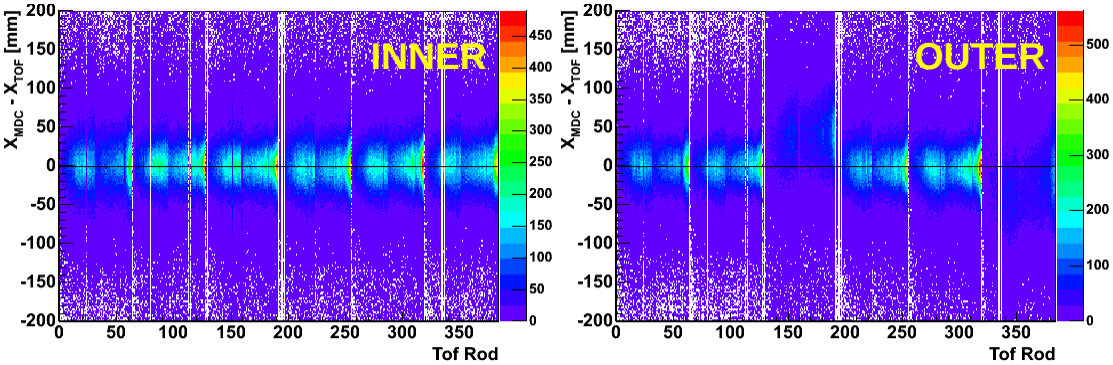

Figure 6.4 – Differences between projected hits (x_{MDC}) and TOF ones (x_{TOF}) in function of the TOF rod number, by using inner (left) and outer (right) segment. Apart from 3 MDC sectors, the distributions are comparable.

The calibration by using inner segment is consistent also for outer segment, but here 3 MDC sectors show systematic shifts of few centimetres respect to the zero value. This is not connected to TOF position but to the poor angular resolution of segment reconstruction by using only one MDC chambers, as shown in chapter 5; the shift is consistent to the one found by analysing elastic scattering channel.

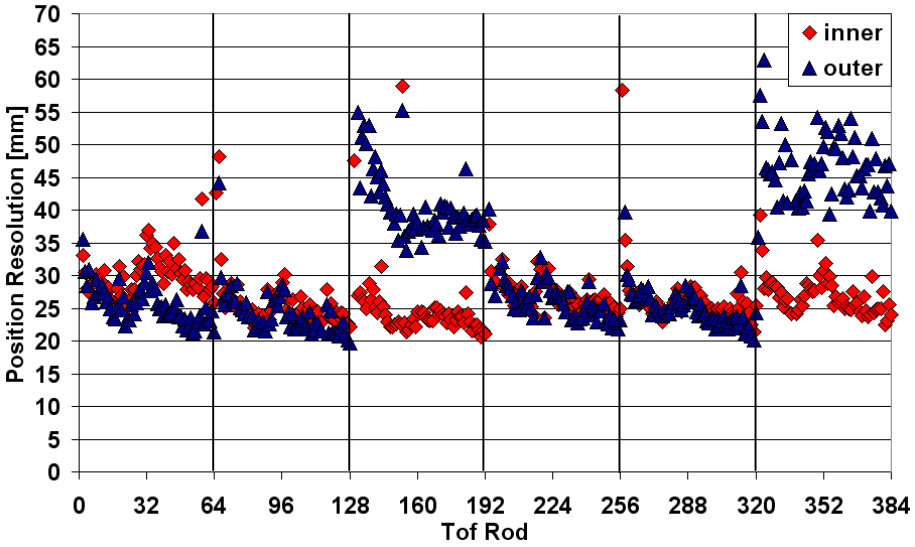

Figure 6.5 – TOF position resolution in function of the rod number, obtained by residual widths for inner and outer segments.

The difference between TOF position and projected one (Figure 6.4) was fitted by a gaussian function for each rod; position offsets are given by the centroids of the distributions, while widths are an estimation of the rod position resolution.

Figure 6.5 shows the obtained width values in function of rod number, calculated separately for inner and outer chambers; the two distributions agree for most of the rods. Three MDC sectors (the 3rd [128-192] and the 6th [320-384]) cannot be compared as already mentioned. In the 1st sector [0-64] outer chambers widths are lower respect to inner ones; this is connected to the low number of working wire layers in MDC plane I, which decreases the quality of angular reconstruction.

The average position resolution for thinner and thicker TOF rods is shown in Table 6-1, and it is about 2.5 cm. We can convert this value into intrinsic time resolution by diving it by group velocity values; using this rough calculation we can estimate a time resolution between 150 ps and 160 ps.

	INNER MDC	OUTER MDC[3]
2x2 cm^2 rods	24.6 ± 1.5 mm	23.5 ± 1.7 mm
3x3 cm^2 rods	26.7 ± 2.6 mm	26.3 ± 2.4 mm

Table 6-1 - Position resolution values for TOF rods.

Group velocities were calculated using a laser system on November 2001, and the obtained average values, which were used in the analysis, were 164 mm/ns for 3x3 cm^2 rods, and 162 mm/ns for 2x2 cm^2 rods.

A cross check of these number can be done after the position offset calculation. After the position calibration, from the formula:

$$x = \frac{1}{2}(t_R - t_L)\cdot Vg + x_{offset} \qquad \text{(Eq. 6-6)}$$

[3] In the average evaluation sectors 3 and 6 were not taken into account, because of the 3 MDC sectors problem.

if we use the position corrected by offset (so $x_{offset} \equiv 0$), we can write the group velocity in function of:

$$Vg = x \cdot \frac{2}{t_R - t_L} \qquad \textbf{(Eq. 6-11)}$$

If we use the known position of the projected hit as x (x_{MDC}), we can plot $x \cdot 2/t_R - t_L$ in function of the tof rod number, as shown in Figure 6.1.

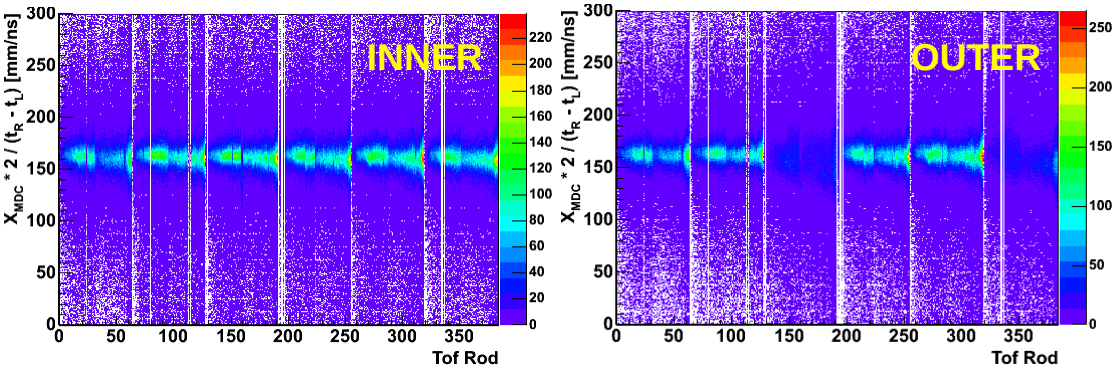

Figure 6.6 – Group velocity evaluation in function of rod number, using inner (left) and outer (right) segment. No systematic deviations are visible (apart from 3 MDC sectors - outer chambers).

The distributions do not show systematic deviations, and they are similar for both inner and outer modules (apart from outer chambers of 3 MDC sectors). The average values are shown in Table 6-2; the obtained values are comparable for inner and outer segments, and to the ones evaluated in November 2001.

	INNER MDC	OUTER MDC[3]
2x2 CM^2 rods	160.5 ± 1.1 mm/ns	161.8 ± 0.9 mm/ns
3x3 CM^2 rods	163.7 ± 1.0 mm/ns	163.9 ± 1.0 mm/ns

Table 6-2 - Average group velocity values for TOF rods.

6.3 Time calibration with START detector (September 2003)

The following procedure is used for all the experiments where a START detector is present, so when the START signal does not depend on the event.

The main idea of time calibration is to use particles which have a well known time of flight. By minimizing the difference between their experimental tof and the predicted one, it is possible to evaluate time offsets for all the time of flight subdetectors.

Electrons (and positrons) can be used to perform time calibration: in the energy range studied by the HADES spectrometer the emitted leptons travel at velocity close to

the light speed; their time of flight does not depend on their momenta but only on the travelled distance between the emission point and the TOF/TOFINO walls.

We can write the electron tof as:

$$tof = \frac{len}{\beta c} \equiv \frac{len}{c} \qquad \textbf{(Eq. 6-12)}$$

where *len* is the travelled path length, β is the electron velocity ($\beta \equiv 1$), and *c* is the light speed. If we assume a path length of 2100 mm (the average distance of META systems from the target), the electron time of flight will be about 7 ns.

Electrons and positrons are selected by angular correlation of the track with the RICH detector, which is hadron blind; the path length is given by the META hit position in the laboratory coordinate system (for no field data) or by the tracking algorithm (for field data); the time of flight is given by TOF and TOFINO walls.

By combining all these data, the time calibration is performed by choosing lepton candidates and calculating their tof normalized to the path length of 2100 mm (by assumption):

$$\overline{tof} = tof \cdot \frac{2100}{len} \qquad \textbf{(Eq. 6-13)}$$

where *tof* is the experimental value and $\overline{tof}$ is the normalized one. In this way $\overline{tof}$ does not depend on travelled distance and we can tune time offsets by setting it at 7 ns.

In the following paragraphs the procedure will be explained step by step, and the resolution values will be presented, obtained by analysing field runs for September 2003 data.

6.3.1 START calibration

The start detector for September 2003 it was constituted by sixteen scintillator stripes of 1x12 cm^2 size. Each one has its electronic chains so one time offset for each channel has to be calculated.

However from the beam profile (see left side of Figure 6.7) we can see projectile particles do not hit all the stripes, so the procedure can be used only for the central ones which have the higher number of counts.

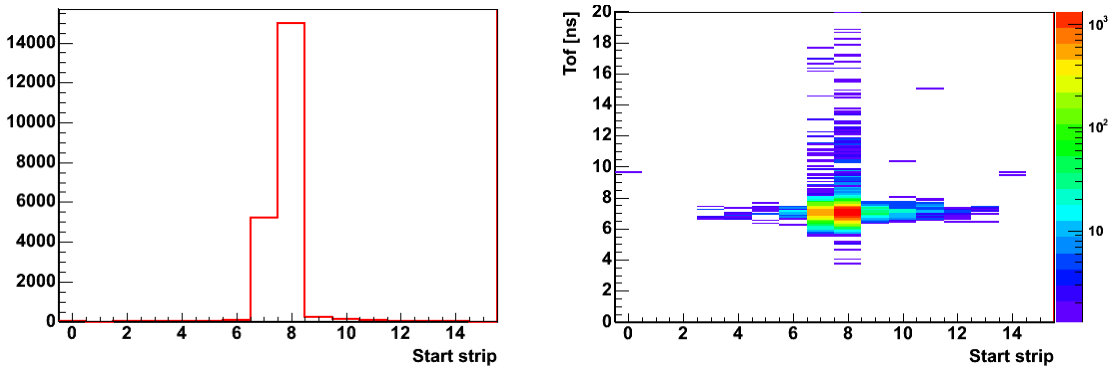

Figure 6.7 – Hit distribution in START stripes (on the left), which corresponds to the beam profile. On the right the normalized tof distribution for lepton tracks in function of the strip number, after calibration procedure.

The initial time offsets for all the stripes are set to zero. To calibrate START we select lepton tracks which hit only one particular TOF rod (in order to not depend on TOF time offsets), and we calculate their normalized time of flight values. For each different stripe we construct tof distributions and we fit the peak by a gaussian function.

If the stripes were calibrated all the peaks should stay at 7 ns position; before calibration this does not happen, so from the difference between peak centroids and the 7 ns assumption we can calculate time offsets stripe by stripe[4].

Figure 6.7 shows the distribution of normalized time of flight in function of the stripe number, after calibration.

After this procedure all the tof values will be corrected by:

$$t^{i}_{START} = t_0 - t^{i}_{offset} \qquad \textbf{(Eq. 6-2)}$$

in order to not depend on START stripes in the later stages of the analysis.

6.3.2 TOF time calibration

After the START detector is calibrated, we can evaluate time offsets for TOF detector.

We select lepton tracks which hit TOF rods, we calculate their normalized tof and fill distributions of time of flight rod by rod. Each distribution is fitted by a gaussian function, and the difference between centroids and the assumed value of 7 ns gives the time offsets for all the rods.

The left plot of Figure 6.8 shows the two dimensional spectrum of normalized tof in function of the rod number after the time calibration. We can see all the time distributions are well placed to 7 ns.

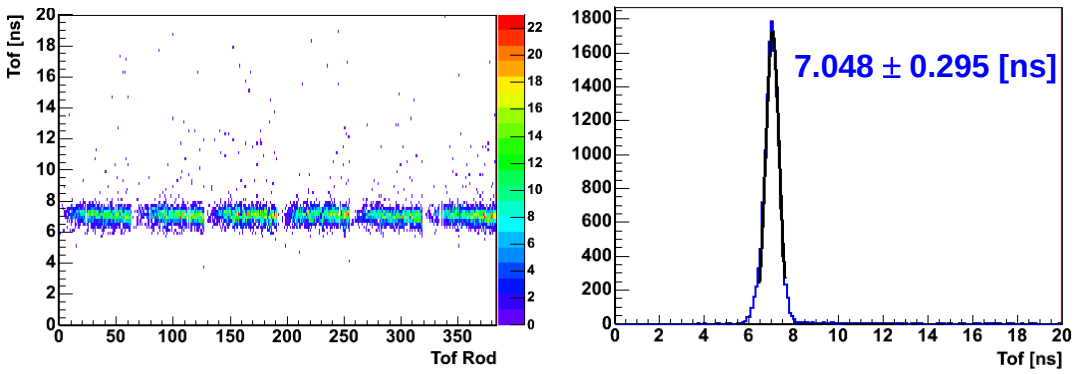

Figure 6.8 – TOF time of flight distributions for leptons, in function of rod number (left) and integrated all over the rods (right). The obtained resolution value (295 ps) is the quadratic sum of TOF and START time resolutions.

Figure 6.8 shows the normalized tof distribution integrated over the whole TOF. By fitting the peak with a gaussian function the obtained centroid stays at 7 ns, and the sigma of the fit gives us an estimation of the average time resolution of TOF detector.

[4] In general, after all the stripe offsets are calculated in this way, by convention we add a constant value to all the offsets, in order to put the offset of the most hit stripe to zero. The time of flight peak will be adjusted to 7 ns in a second step after TOF and TOFINO calibration.

The obtained resolution value of 295 ps is larger than what expected from position calibration. Indeed the tof measure is given by the subtraction of STOP time minus START time:

$$tof = t_{STOP} - t_{START} \qquad \text{(Eq. 6-1)}$$

so the tof resolution depends even on START detector resolution, according to:

$$\sigma_{tof} = \sqrt{\sigma_{STOP}^2 + \sigma_{START}^2} \qquad \textbf{(Eq. 6-14)}$$

In order to obtain a value independent on START detector we can use dilepton pairs.

If we have two leptons emitted in the same event, we can make the difference of their normalized time of flight values t_i. If we consider that for both particles the t_{START} is the same, the difference can be simply expressed as:

$$\Delta tof = t_2 - t_1 \qquad \textbf{(Eq. 6-15)}$$

and the resolution of the time difference is correlated to the single TOF resolution by:

$$\sigma_{\Delta tof} = \sqrt{\sigma_{t_2}^2 + \sigma_{t_1}^2} \equiv \sqrt{2} \cdot \sigma_{TOF} \qquad \textbf{(Eq. 6-16)}$$

by assuming $\sigma_{t^1} \equiv \sigma_{t^2} \equiv \sigma_{TOF}$.

From the tracking system we can have the information about the charge polarity of the particle which crosses our spectrometer, from the trajectory deviation inside the magnetic field. We can select events which contain lepton pairs of opposite charge, and plot their difference in time of flight (Figure 6.9).

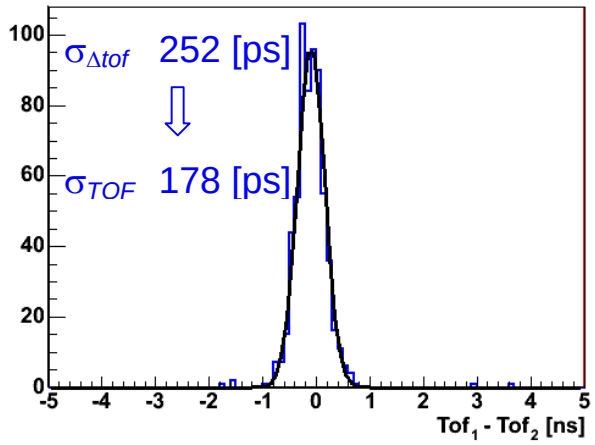

Figure 6.9 – Time of flight difference for dileptons both in TOF system.

From the fit over the tof difference we obtain a width of 252 ps. By dividing this number by $\sqrt{2}$ we obtain a TOF time resolution of 178 ps, which is the typical value for rods after good calibration.

After we have the intrinsic TOF time resolution, we can derive the value for the START detector. By combining equation 6-14 and the obtained σ_{tof} of 295 ps, we obtain a START time resolution of about 235 ps.

6.3.3 TOFINO time calibration

The procedure performed for TOFINO calibration is the same of what was used for TOF system.

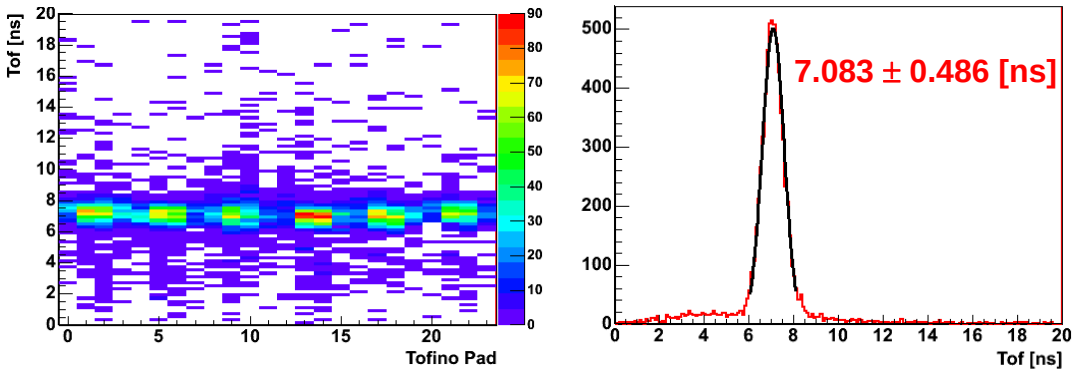

Figure 6.10 - TOFINO time of flight distributions for leptons, in function of pad number (left) and for all over the pads (right), after TOFINO time calibration.

In Figure 6.10 the distributions of TOFINO time of flight values (normalized) are plotted after the calibration, in function of the TOFINO pad number on the left (one sector is made by four pads) and for the whole system on the right.

The obtained resolution value from the fit (486 ps) includes the effect of START detector; by the squared subtraction of this value minus the START resolution, as for TOF detector, we can evaluate an intrinsic TOFINO time resolution of 425 ps.

In the analysed data sample there are not so many dilepton pairs where both the particles hit the TOFINO region, as shown in Figure 6.11.

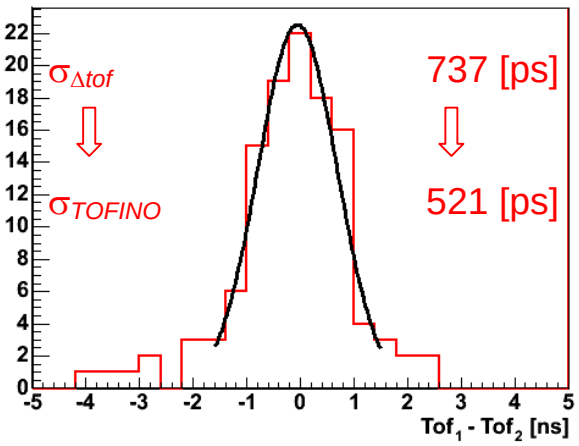

Figure 6.11 – Time of flight difference for dileptons both in TOFINO system. The small number of counts in the distribution does not allow to provide reasonable fit values.

The peak was fitted by a gaussian function, but the width estimation has large errors connected to limited statistic, so the only affordable value of intrinsic time resolution is 425 ps calculated by single leptons analysis.

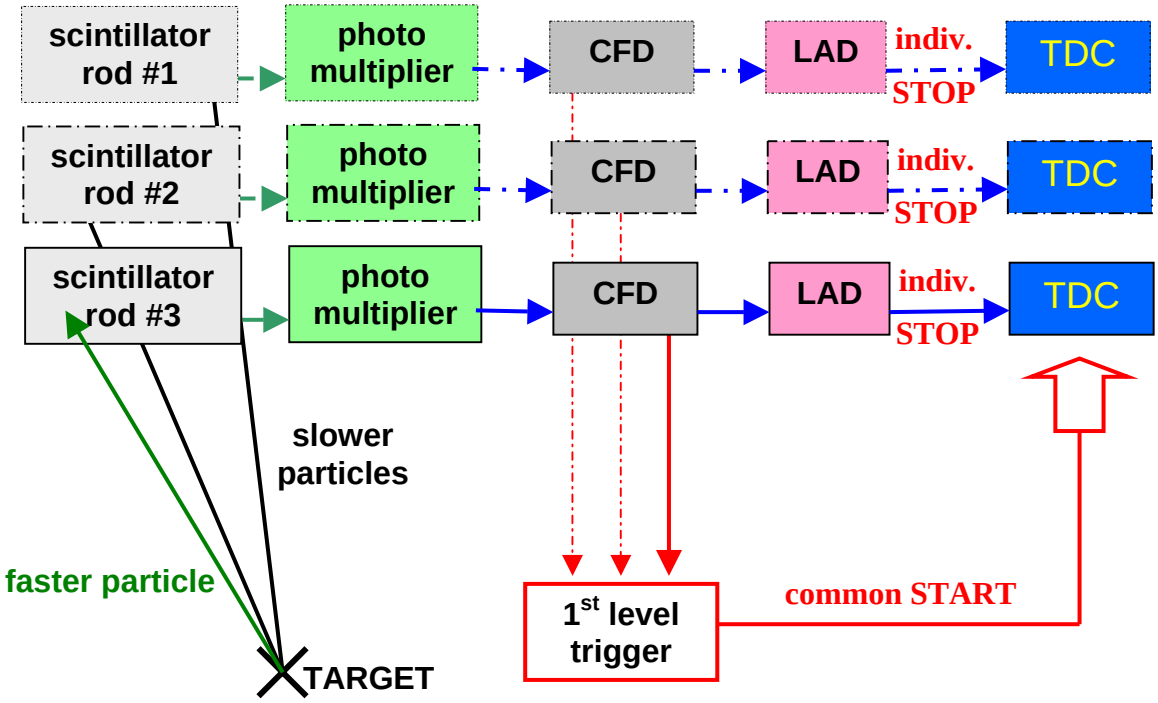

Figure 6.12 – Principle of tof measure without START detector. The faster particle which hit a META pad gives the START to time of flight measure.

6.4 Time calibration without START detector (January 2004)

In the January 2004 experiment the START detector was not used as time reference, because of the high number of secondaries produced by itself. This means there was not a common start time for tracks in the same event, but in general the data acquisition was started by the fastest particle which crossed the TOF/TOFINO walls and produced a signal above TDC thresholds (see Figure 6.12).

Let assume in a nuclear collision a particle is emitted from the target, crosses the spectrometer and produces a light signal in the scintillator rods. The time between the instant when the reaction occurred and when the particle hit the TOF detector is called time of flight (*tof*). The light travels towards the photomultiplier and it is converted into an electronic signal, reaching the TDCs after a time τ given by:

$$\tau = tof + \frac{x}{Vg} + offset \qquad \textbf{(Eq. 6-17)}$$

where *offset* is the time offset of the electronic chain (due to electronics, delay modules, cable length, and so on).

TDCs measure the time between a START and a STOP signal. If the acquisition is started from the *"0"* particle, the measured time $\underline{t}^i$ of the *i*th particle will be expressed as:

$$\underline{t}_i = \tau_i - \tau_0 = tof_i - tof_0 + \frac{x_i}{Vg_i} - \frac{x_0}{Vg_0} + offset_i - offset_0 \qquad \textbf{(Eq. 6-18)}$$

where $offset_i$ are the offsets due to the STOP chain, while $offset_0$ is connected to the START chain and the 1st level trigger.

By knowing hit point positions, group velocities and offsets, we can see our measured time does not correspond to the "real" time of flight, but instead to the difference in time respect to the faster electronic signal.

In the case of TOF rods we obtain a measured time t_{TOF} given by:

$$t_{TOF} = \frac{1}{2}\left(\underline{t}_R + \underline{t}_L\right) = tof_{TOF} - tof_0 + offset_{TOF} - offset_0 \qquad \textbf{(Eq. 6-19)}$$

while for TOFINO we must correct the measured time by the *x* distance between the hit point and the PMT given by the SHOWER detector. Generally we obtain:

$$t_{TOFINO} = \underline{t}_{TOFINO} - \frac{x_{TOFINO}}{Vg_{TOFINO}} = tof_{TOFINO} - tof_0 + offset_{TOFINO} - offset_0 \qquad \textbf{(Eq. 6-20)}$$

assuming t_{TOFINO} contains even the distance correction.

The TOF position information is substantially unaffected by this different kind of measure, because it is based on left/right time difference and it does not depend on the particles which started the acquisition (no dependence on $offset_0$).

The time calibration is more complicated because we cannot use single lepton time as we usually do in experiments with START detector; in this case we miss the information on the time of flight of the particles which started the acquisition (we know only the time difference respect to it).

We can divide the time calibration procedure in two steps; first we calculate the time offsets of TOF/TOFINO pads, and after the start time of the reaction event by event.

In order to calculate time offsets we need to use well known time differences. We can take pairs of identified particles, whose theoretical time of flight can be estimated from momentum and mass values, calculate their experimental difference in time and compare this value to the theoretical one. In this way we can tune time offsets in order to have coherent tof values for all the pads of TOF and TOFINO walls.

To perform this kind of calibration we can be use alternatively dilepton pairs or pp elastic pairs.

It is possible to use the RICH information to select pair of leptons in the same event, as shown in 6.3.2. Their theoretical time of flight is well known (high energy leptons travel close to the light speed), but their production rate is lower respect to other hadronic processes.

Proton-proton pairs can be easily identified by selecting positive charged tracks (from the trajectory deviation inside the magnetic field) and doing a selection on the angular variables, as shown in the previous chapter; the elastic channel cross section is quite high, but elastic protons cover a limited region of the polar angle (below 60°), so

they do not hit all the TOF rods; moreover the theoretical time of flight of the protons has to be calculated from momentum, and it depends even on the tracking resolution.

For these reasons dilepton pairs were chosen as more suitable tool for the time calibration.

6.4.1 Calibration with dileptons

Electrons and positrons with energies above few MeV travel at velocities close to the light speed. This means they should have the same velocity, so they should cover the same path length in the same time.

If we consider a pair of leptons emitted in the same collision, their time of flight normalized to the same path length (calculated by the tracking algorithms) t_1 - t_2 should be centred at zero:

$$0 \equiv t_1 - t_2 = \underbrace{tof_1 - tof_2}_{0} + offset_1 - offset_2 \qquad \textbf{(Eq. 6-21)}$$

where now the offsets are only connected to the STOP chain.

By angular correlation between RICH and MDCs we select dilepton pairs; the tracking algorithms are able to estimate the track path length, and the sign of the charge by trajectory deviation in magnetic field region. From all these informations we can tune the offsets of a pad respect to the offset of another pad.

By considering that this calibration consists on calculating only relative offsets (the global one has to be calculated event by event and it will be explained in 6.5), we must calibrate TOF and TOFINO systems separately. The adopted procedure is the following:

1. Calibration of TOFINO pads respect to one TOF rod (sector wise);
2. Calibration of TOF rods respect to TOFINO pads (sector wise);
3. Calibration of offsets between different sectors.

A first analysis was run with the full statistic of January 2004 using the September 2003 parameters; in between the two experiments no cables and no electronic modules were changed, so the September offsets should be close to the good ones, but they need to be refined in order to achieve the correct time resolution.

The following paragraphs will explain the calibration steps and the obtained results, using Runge Kutta as tracking algorithm. After this calibration procedure the time difference of dileptons was calculated to obtain an estimation of the time of flight resolution.

6.4.2 TOFINO offsets

The first step consists on calibrating TOFINO pad offsets respect to other pads in the same sector.

The best way to perform this calibration consists on choosing pair of lepton tracks in the same event, of opposite charge, where one particle hits a TOF rods and the other a TOFINO pad of the same sector. If we select this kind of pairs, but where the TOF particle hit always only one fixed rod (one for each sector), we can calculate the two particles difference in time (normalized to the same path length), and adjust TOFINO offsets pad by pad relatively to the chosen TOF rod, by setting this difference to zero value.

In this case we are calculating TOFINO offsets respect to the selected TOF rod. We use only one determined rod different for each sector, in order that our offset determination is not influenced by superimposition of different TOF rods with not tuned time offsets.

After this offset calculation, Figure 6.13 shows the difference in time (normalized to a path length of 2100 mm) between TOF-TOFINO lepton pairs in the same event belonging to the same sector versus TOFINO pad number (4 pads correspond to one sector), where it was hit only one determined TOF rod, different for each sector.

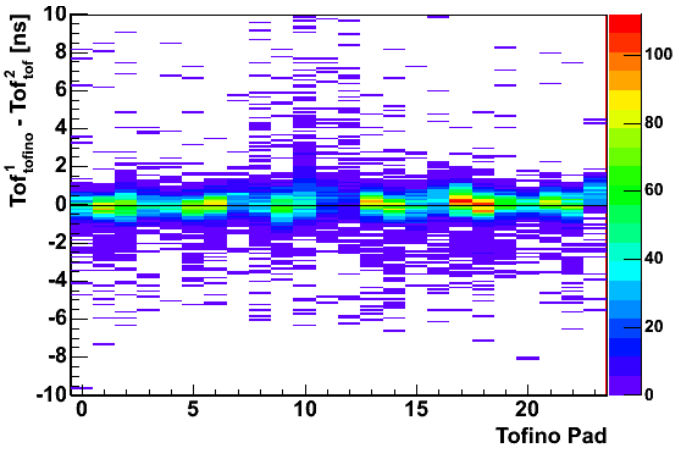

Figure 6.13 – Time difference of dilepton pairs (TOF-TOFINO) versus TOFINO pad number, after TOFINO offsets tuning.

After the TOFINO calibration all the time distributions are placed in the same position. This means TOFINO pads on the same sector are well calibrated respect to each other, but if we compare pads belonging to different sectors, the time difference will depend on the offsets of TOF rods used for this calibration.

Therefore, after TOFINO calibration, we need to tune TOF offsets.

6.4.3 TOF offsets

The same kind of procedure was adopted for TOF rods. After selecting pairs of leptons in the same event, in the same sector and hitting both TOF and TOFINO systems, we can calculate the time difference of the two tracks, this time using as TOFINO values the times corrected by the previous paragraph procedure. In this case we do not use one single TOFINO pad for each sector, because we assume pad offsets are well tuned by the first step of the calibration.

Figure 6.14 shows the time difference for TOF-TOFINO lepton pairs in function of the TOF rod number, after the correction of TOF offsets.

The time differences are well centred to zero value, but we can see a second structure in the low polar angle region (higher rod number for each sector). The secondary peak is displaced of about -2 ns respect to the expected position.

This peak is present in all the days of beam, and it is not connected to an offset movement due to some effects of electronics. By analysing files from simulation it was found the same behaviour, and it was understood its origin.

In all the pairs with the 2nd peak, the positron hit a TOFINO pad and its real time of flight correspond to a value of about 5 ns, so below the correct value of 7 ns of a particle travelling at the light speed. This can happen when more than one particle hit

the same TOFINO pad; in this case one of the two particles will have a wrong time (in general lesser than the correct value).

This effect is secondary so it can be neglected, and it does not harm the time calibration. For the effected rods the fitted time peak is the primary one.

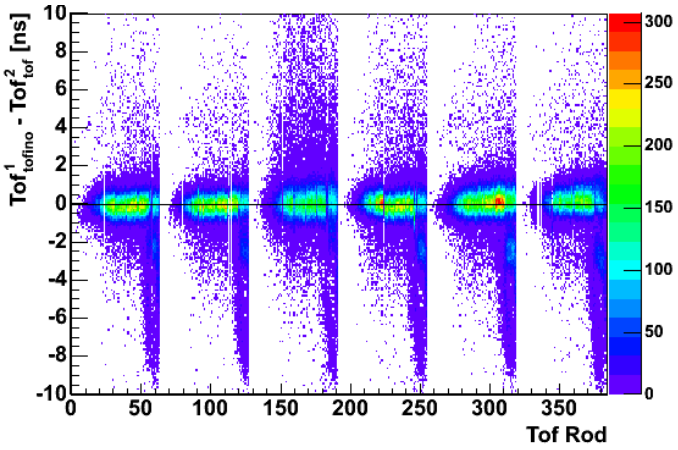

Figure 6.14 – Distribution of dilepton pairs (TOF-TOFINO) time differences versus TOF rod number, after TOF offsets tuning.

6.4.4 Inter sectorial calibration

After the first two steps of the calibration procedure all the pads of each sectors are well tuned respect to each other pad in the same sector. The final step consists on aligning in time all the sectors, so calculating a global offset for each sector respect to a well determined one (the reference sector).

We choose dilepton pairs hitting two neighbour sectors, using only TOF system because of its better time resolution, and we impose their time differences to zero; in this way the offsets are calculated respect to the previous sector, and of course the sum of all their values is close to zero.

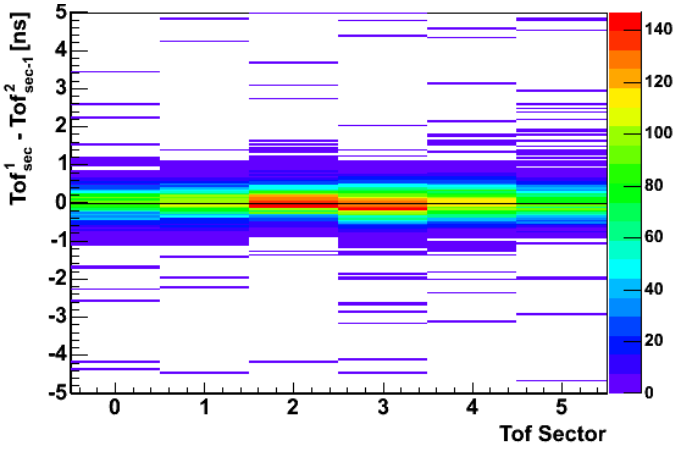

Figure 6.15- Time difference of dilepton pairs belonging to neighbour sector, after the last step of time calibration.

Figure 6.15 shows the final plot after this procedure. It was decided to leave the 6th sector unchanged (number #5 in the plot), and to calculate the other sector offsets respect to it.

6.4.5 Time resolution

After the calibration is concluded it is possible to evaluate the time resolution obtained, using dilepton pairs as before.

If we consider a pair of leptons we can plot their difference in time of flight $\Delta tof = t_1 - t_2$, and fit the distribution by a gaussian function. In this case the peak should be centred to zero, while the sigma of the gaussian is an estimation of the time resolution, given by:

$$\sigma_{\Delta tof} = \sqrt{\sigma_{t_1}^2 + \sigma_{t_2}^2} \qquad \textbf{(Eq. 6-22)}$$

where σ_{t_1} and σ_{t_2} are the resolution values of single time of flight measure.

If we choose pairs belonging to the same system, we can easily estimate the intrinsic time resolution of TOF and TOFINO detectors by the formulas:

$$\sigma_{TOF} = \frac{\sigma_{TOF-TOF}}{\sqrt{2}} \qquad \textbf{(Eq. 6-23)}$$

$$\sigma_{TOFINO} = \frac{\sigma_{TOFINO-TOFINO}}{\sqrt{2}} \qquad \textbf{(Eq. 6-24)}$$

In Figure 6.16 we can see the time difference distribution between leptons which both hit TOF detector. The width of the distribution is 309 ps, which corresponds to a TOF intrinsic time resolution of about 219 ps. This value is higher respect to the one obtained for September 2003 (178 ps) but the difference is not so much, and considering the different and much complicated procedure which was used to obtain the offset calibration, using different measures with different systems, it is not possible to decrease further this number with this method for January 2004 experiment.

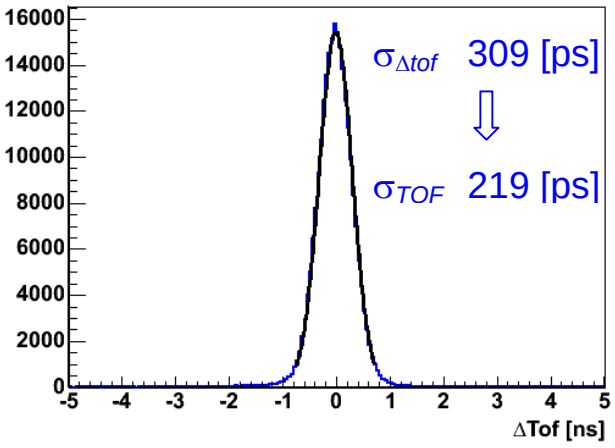

Figure 6.16 - Time difference distribution of leptons which both hit TOF detector.

Figure 6.17 shows the same distribution for TOFINO-TOFINO pairs. In this case the obtained width value for time difference fit is 704 ps, which corresponds to a TOFINO intrinsic time resolution of about 498 ps. If we compare this number with the one obtained in September 2003 (425 ps), even for TOFINO we are close the values obtained by the "usual" single track procedure.

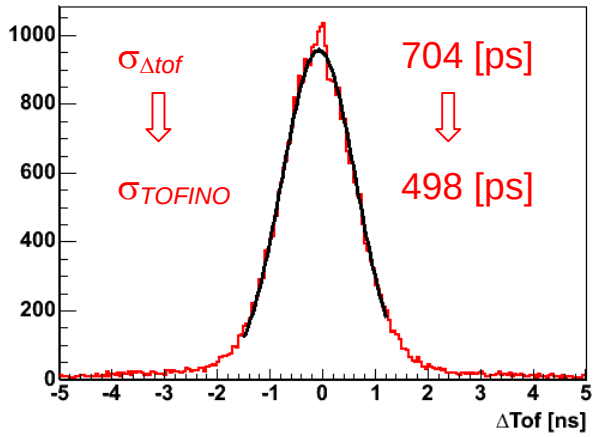

Figure 6.17 - Time difference distribution of leptons which both hit TOFINO detector.

The January 2004 experiment was the first time the START detector was not used; the described procedure was developed for this occasion and never tested before. The obtained resolution values are close to the one calculated by using data with START detector, and this means that the procedure is under control and it provides good results that can be used for the analysis.

After that single pad time offsets are calculated, the start time of the reaction is needed.

6.5 Start time reconstruction

As previously stated, in the experiments were START detector is not present the TOF/TOFINO systems do not measure the particle time of flight, but its difference in time respect to the particle which made the acquisition start. In this case we need to reconstruct the start time of the reaction event by event, in order to have the correct time of flight for all the particles.

To perform this kind of job an algorithm was developed and it will be explained in the next paragraph. The capability and the resolution of the method were explored first by studying simulation data, and after by experimental data taken in September 2003 beam time, when the hodoscope detector was present.

At last the capability of this algorithm for January 2004 data will be shown.

6.5.1 The algorithm

From the considerations of the previous chapters, the time of flight (*tof*) of a particle is given by the sum of its experimental time (t) measured by the TOF/TOFINO wall plus the time-of-flight (tof_0) of the particle which started the acquisition:

$$tof = t + tof_0 \qquad \textbf{(Eq. 6-25)}$$

In order to avoid the dependence on the faster particle, we can simply consider the time difference of any two particles produced in the same event; from the previous equation we can easily obtain the relation:

$$tof_1 = tof_2 + t_1 - t_2 \qquad \textbf{(Eq. 6-26)}$$

It follows that if we want to know the time of flight value of all the particles inside an event we need to know first the tof of a single particle, and after we can recalculate the tof of all the other ones.

Let assume we have a particle whose momentum (*p*) and track length (*len*) are measured by the tracking algorithm; we can calculate the theoretical time of flight of the particle by the formula:

$$tof = \frac{len}{c}\frac{1}{\beta} = \frac{len}{c}\frac{\sqrt{p^2 + m^2}}{p} \qquad \textbf{(Eq. 6-27)}$$

where *c* is the light speed and *m* is the mass of the particle. If we can identify a particle inside the event we can assume its mass, we can calculate its theoretical time of flight, and from this value we can recalculate even the tof of all the other particles in the same event.

The strongest particle identification algorithm of the HADES spectrometer consists on the simultaneous measure of momentum and β of the particle, but of course it cannot be used before the start time is reconstructed. Nevertheless there are other methods, independent from the time measure, that can be adopted.

The first one is the lepton identification by RICH detector. If we select tracks which are correlated in angles to a ring in the RICH detector, we can assume they are electrons or positrons.

On a second step, we can select negative charged tracks (from the trajectory deviation inside the magnetic field) which are not correlated to RICH detector, and so that were not identified as electrons; in this case we can assume these tracks are negative pions.

For all the events where these kinds of identification are not possible, events with only positive charged tracks, we cannot do any assumption on the identity of the particles (they can be both protons or pions), so this method is not usable for them.

But it is important to stress the reactions of interest are the decay channels of η meson, so $pp \rightarrow pp\pi^+\pi^-\pi^0$ (hadronic) and $pp \rightarrow ppe^+e^-\gamma$ (electromagnetic); events with only positive tracks are not interesting for this analysis, or we are able to use other kinds of identification (such as the elastic channel selection described in the previous chapter).

By identifying a particle in the event, which do not need to be the faster one, we can assume its mass and so calculate its theoretical time of flight as previously explained. By the difference of the experimental value (t_{exp}) and the theoretical one (t_{teo}) we can finally calculate the start time of the reaction, by the formula:

$$tof_0 = t_{teo} - t_{exp} \qquad \textbf{(Eq. 6-28)}$$

and we can add this value to the measured time of the other particles inside the same event, to obtain the corrected time of flight by equation 6-25.

To summarize the procedure Figure 6.18 and Figure 6.19 show flowcharts of the algorithms used for the start time reconstruction and the particle identification.

The algorithm was tested with simulation data, where the particle tof is known. After it was evaluated a good response, it was used in experimental data of September 2003 run, where the START detector was present and so a good time of flight reference.

At last it was used in January 2004, showing its capability to make possible particle identification even without the START detector. All these steps will be studied in the next paragraphs.

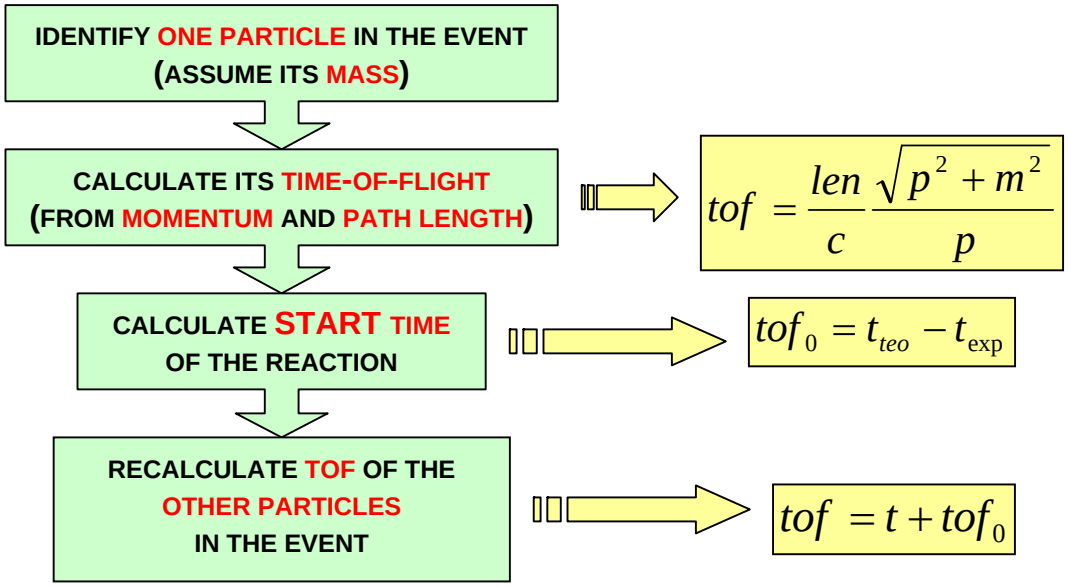

Figure 6.18 – Flowchart of the algorithm used for start time reconstruction.

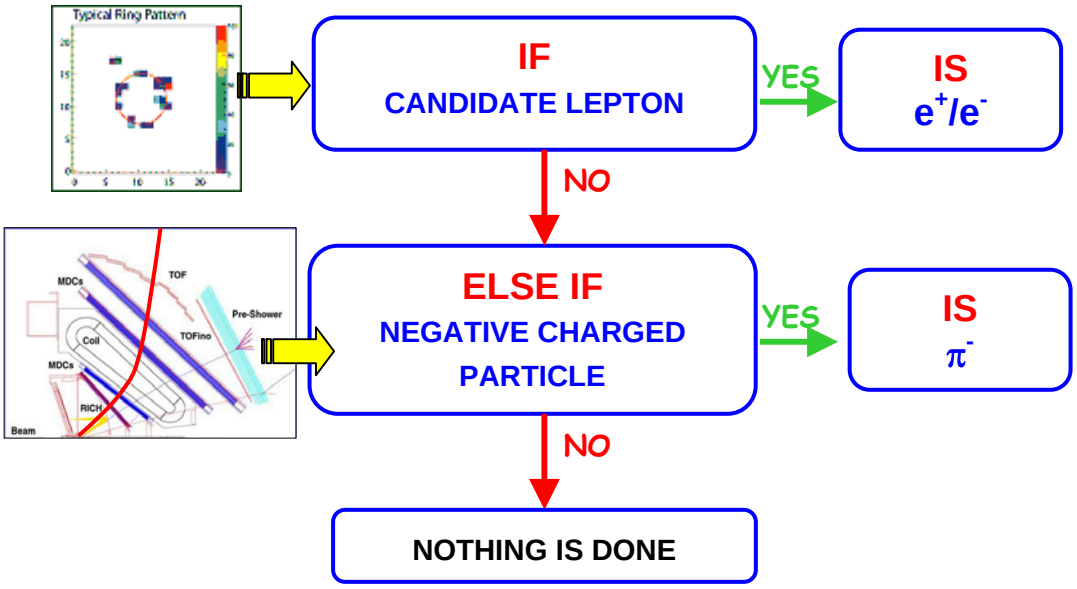

Figure 6.19 – Schematic view of the particle identification method used for start time reconstruction.

6.5.2 Simulation

Figure 6.20 shows the two dimensional plot of momentum times polarity versus β for simulation data. All the particles are placed in well defined regions of the plot, and by applying appropriate selection particle identification can be done. We want to use the same identification procedure even for the January 2004 experiment, when the START detector was not present, so we need start time reconstruction.

In simulation the START detector is not included, all the particles have the same start time without any spread of resolution; the only resolution effects are included inside TOF and TOFINO measured values. This means we can apply the start time reconstruction algorithm to simulated data, and compare the original time of flight value to the reconstructed one, in order to evaluate resolution and efficiency of the method.

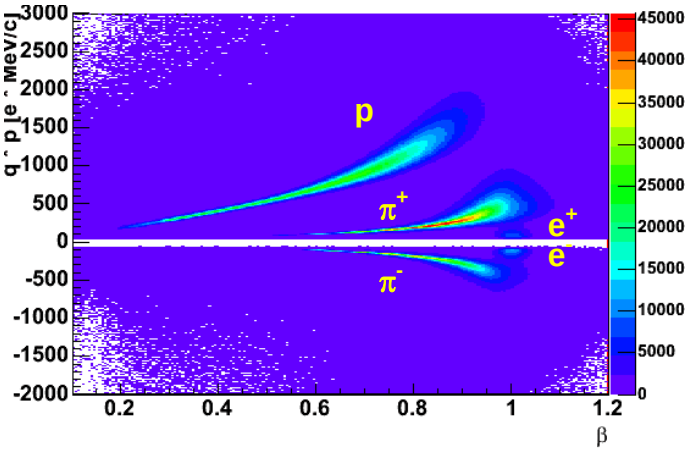

Figure 6.20 – Momentum times polarity versus β spectra for simulation data, by using original tof values. All the particles are placed in well defined regions of the plot.

If we consider a particle whose tof was reconstructed, we can express this value tof_{rec} by the formula:

$$tof_{rec} = tof_{\exp} + \underbrace{start}_{tof^{0}_{rec} - tof^{0}_{\exp}} = tof_{\exp} + tof^{0}_{rec} - tof^{0}_{\exp} \qquad \textbf{(Eq. 6-29)}$$

where $tof_{\exp}$ is its measured time of flight, *start* is the calculated start time, tof^{0}_{rec} and $tof^{0}_{\exp}$ are respectively the reconstructed tof and the measured one for the particle which we are identifying.

By plotting the difference between reconstructed tof and measured one $tof_{rec} - tof_{\exp}$ we can estimate the resolution of the so calculated start time.

Figure 6.21 shows the time difference distributions, for only identified particles in lepton identification case, in function of momentum times polarity (to distinguish between electrons and positrons), separately for TOF and TOFINO systems.

The distributions are well centred to zero value as expected, but for some tracks the algorithm failed; in simulation we can check the real ID of the track and understand what went wrong.

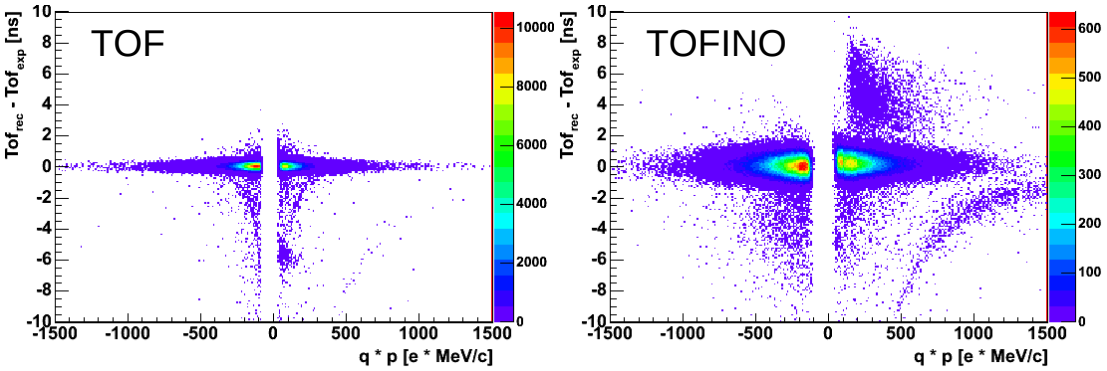

Figure 6.21 – Distributions of differences between reconstructed and measured values of tof for simulation, in cases when a electron/proton is identified (TOF wall on the left side, TOFINO on the right).

In TOF system the noise is negligible and it comes mainly from fake tracks or misidentified pions. In TOFINO system the main sources of errors come from positive charged tracks; in the region of positive differences the bump comes from TOFINO multiple hits: when more than one particle hit the same TOFINO pad, the time measure is affected and it can give tof wrong values (lower even of 6 ns); in the region of negative differences we can see clearly the region made by protons correlated by chance to RICH hits (most of the protons goes to lower polar angles).

Figure 6.22 shows one dimensional distributions of time differences for identified tracks, in the cases of lepton ID. By fitting the peaks by a gaussian function, from the width we can estimate the start time resolution, which is 162 ps for TOF system and 489 ps for TOFINO; these numbers are substantially the time resolution values of the two detectors, because electrons time of flight at these energies does not depend on momenta ($\beta \sim 1$).

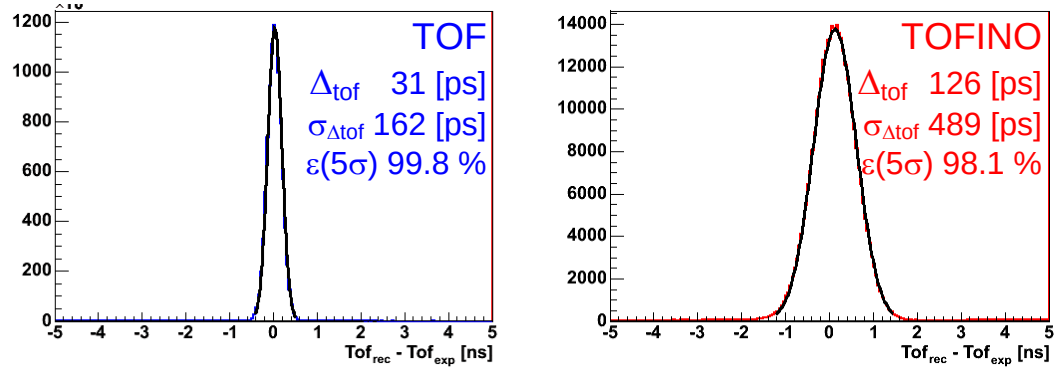

Figure 6.22 – Difference between reconstructed time of flight and measured one, for identified tracks using lepton ID in simulation data (TOF on the left, TOFINO on the right). The reported numbers are the fit values and the efficiency in a 5 σ window.

In order to evaluate the efficiency of the start time so reconstructed, to understand how many times the time recalculation fails, we can check the ratio ε between how many tracks have a time difference inside a 5 σ cut window respect to the total number of reconstructed tracks. In the regions far from the main peak all the contributions should come from tracks with a wrong start time value. The obtained values are reported in Figure 6.22, and are 99.8 % for TOF detector and 98.1 % for TOFINO. The lose in efficiency is almost negligible.

Figure 6.23 shows the momentum times polarity versus β plots for all the particles, in events where the start time was reconstructed by lepton identification (in logarithmic scale); on the left the time used was the original one, while on the right we can see the reconstructed velocity values.

In the plot of reconstructed tracks the vertical line is constituted by identified tracks, which have β≡1 by the algorithm assumption. About all the other particles, we can see pions and protons are well separated and placed in the correct positions, so the particle identification can be still done using momentum versus β method even with reconstructed values.

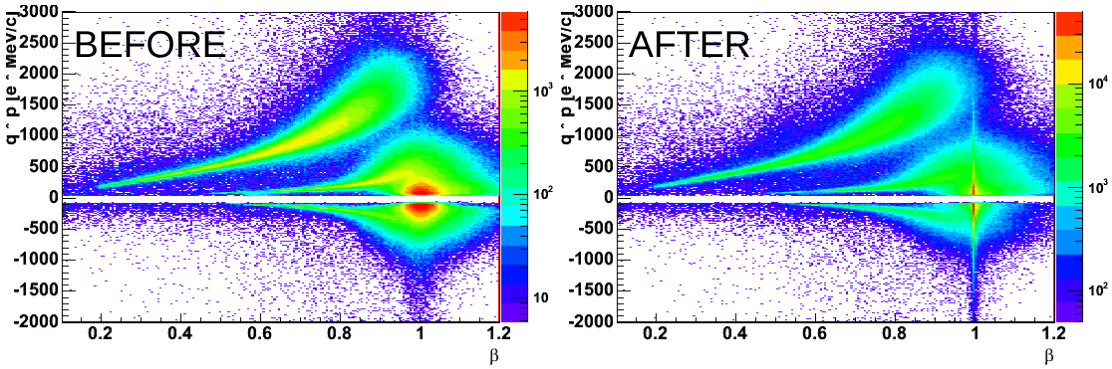

Figure 6.23 – Momentum times polarity versus β spectra before (left) and after (right) start time reconstruction, by identifying an electron/positron in the event (simulation).

The same analysis can be done for events where a negative pions is identified.

Figure 6.24 shows the time difference distributions in function of momentum values. Apart from the main peak centred at zero, we can see there are some deviation for positive difference values. The problems comes from electrons which are not seen by RICH detector and so that are misidentified as pions; in this case the reconstructed tof is greater than the real one (which is almost 7 ns), and it follows a well defined line as it is possible to see in the low momentum region.

By looking at one dimensional distributions (Figure 6.25) the resolution values are a bit higher (192 ps for TOF, 506 ps for TOFINO) respect to cases of lepton identification, because momentum plays an important role in the start time evaluation, and then the measure is affected by its resolution. Moreover while the TOFINO efficiency remains stable at 98.5 %, the TOF one feels the effect of lepton misidentification and it is reduced to 85.1 %.

If we look into the momentum versus β plots shown in Figure 6.26, even when start time is reconstructed from identified negative pion the proton and the pion regions are well defined and separated, and particle identification can be done. In the plot after the start time reconstruction, the red line corresponds to the identified pions, whose time of flight is calculated in function of momentum and so its distribution follows a well defined narrow line.

Another way to check the quality of the start time reconstruction is by looking at the mass values M of the particles, which are connected to their momentum p and velocity β by the formula:

$$M = \frac{p}{\beta}\sqrt{1-\beta^2} \qquad \textbf{(Eq. 6-30)}$$

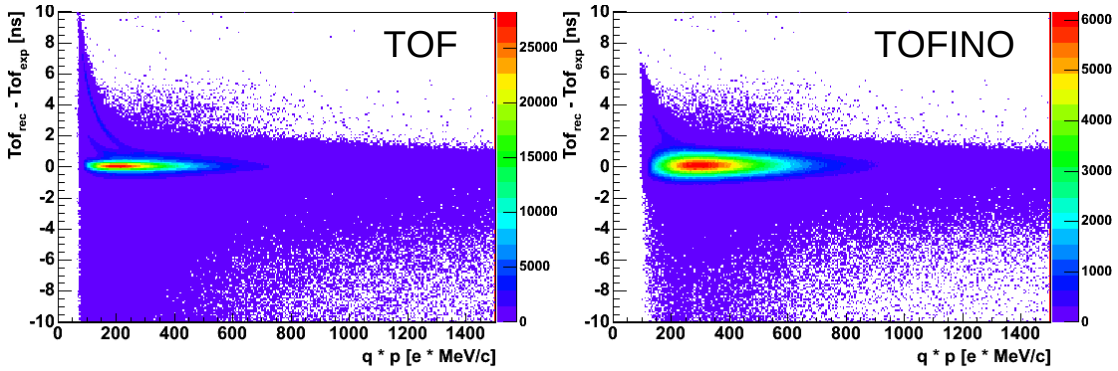

Figure 6.24 – Distributions of differences between reconstructed and measured values of tof (simulation), in cases when a negative pion is identified (TOF wall on the left side, TOFINO on the right).

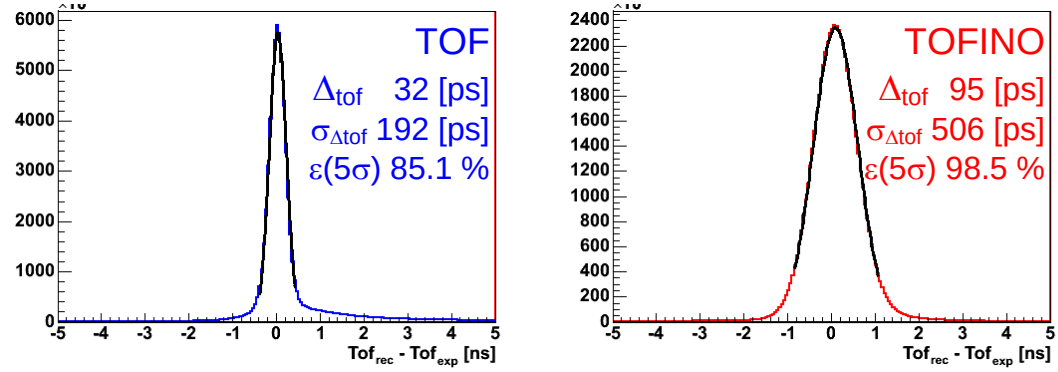

Figure 6.25 – Plots of differences between reconstructed tof and measured one for identified negative pions in simulation, for TOF (left) and TOFINO (right) systems. The TOF distribution has a tail at positive values, connected to electron misidentification.

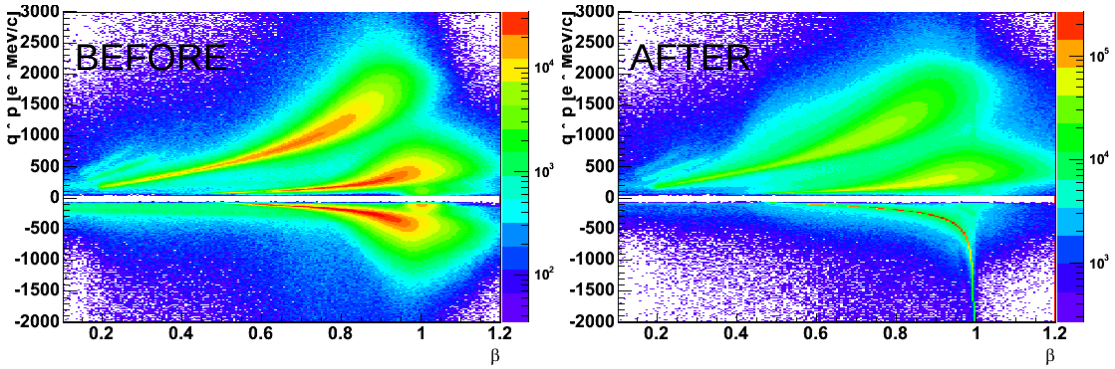

Figure 6.26 – Momentum times polarity versus β spectra before (left) and after (right) start time reconstruction, by identifying a negative pion (simulation).

Figure 6.27 shows the mass distribution (multiplied by charge) of single particles before and after the start time reconstruction, separately for lepton and pion identification. In the spectra all the tracks which were used to reconstruct start time are not plotted, because they have an imposed mass value (only one bin of the histograms) and they cannot be compared to the measured one (which is smeared by detector resolution).

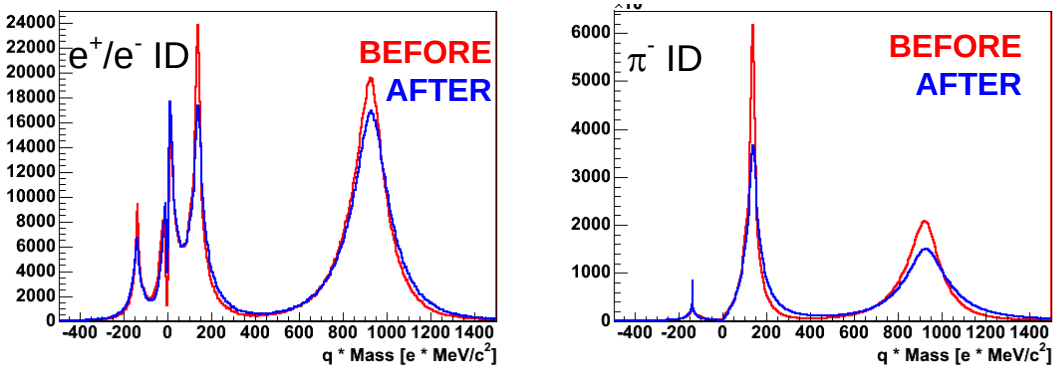

Figure 6.27 – Comparison between single particle mass distributions before and after start time reconstruction (simulation). All the identified tracks are removed from the sample (see the text).

The positions of the mass peaks are centred to the correct values of corresponding particle (so at pion and proton masses), while the widths are a bit broader because of the loss in resolution from the algorithm.

However we can see in simulation the start time is reconstructed in the proper way, and the recalculated time of flight values can be used for particle identification.

In the following paragraph the same analysis will be done for experimental data.

6.5.3 September 2003 data

In September 2003 the START detector was present because the acquisition was operated at lower beam intensity. This means the measured time of flight can be used as reference to evaluate the start time reconstruction for real data.

The time calibration was performed as explained in paragraph 6.3, and the TOF/TOFINO time resolution values are almost the same of what is used in simulation. But in this case there is even the START detector which made the acquisition start, so all the time measures t_{exp} are affected even by its resolution of about 235 ps. We should expect broader time resolution values according to this effect.

Indeed if we consider the relations:

$$start = tof_{rec} - tof_{\exp}, \quad tof_{\exp} = t_{\exp}^{STOP} - t_{\exp}^{START} \qquad \textbf{(Eq. 6-31) (Eq. 6-32)}$$

by propagating errors we find the resolutions values σ are correlated by this formula:

$$\sigma_{start}^2 = \sigma_{rec}^2 + \sigma_{\exp}^2 = \sigma_{rec}^2 + \sigma_{STOP}^2 + \sigma_{START}^2 \qquad \textbf{(Eq. 6-33)}$$

where $t_{\exp}^{STOP}$ and $t_{\exp}^{START}$ are times of the stop (TOF/TOFINO walls) and start (hodoscope) signals in TDCs, and as σ resolution values we indicate: *start* for the reconstructed start time, *res* for the method (so resolution of the time reconstruction from momentum), *STOP* for TOF/TOFINO detectors and *START* for the hodoscope.

Figure 6.28 shows the time differences in function of momenta in the cases of lepton identification. The analysed sample was smaller respect to simulation data, but all the noise sources are still visible even here.

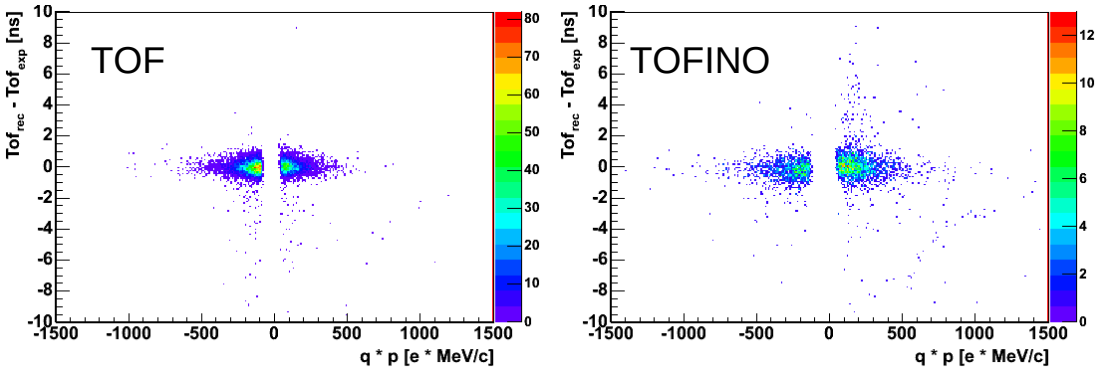

Figure 6.28 – Distributions of differences between reconstructed and measured values of tof (September 2003 data), in cases when a lepton is identified (TOF on the left, TOFINO on the right).

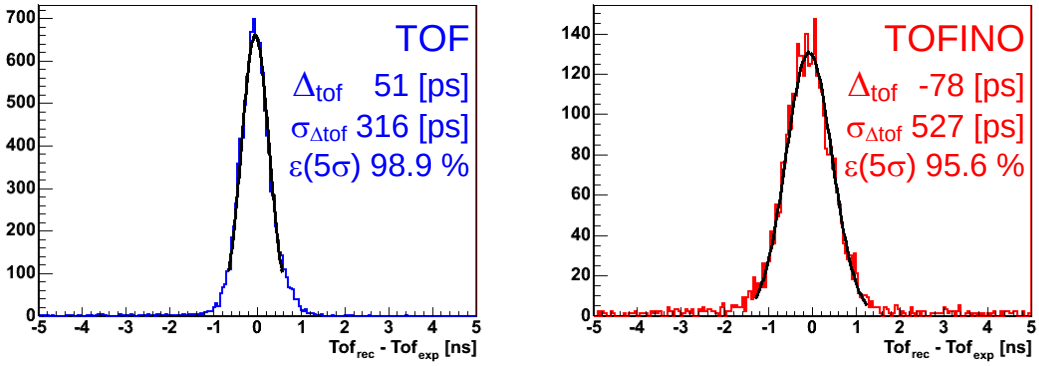

Figure 6.29 – Difference between reconstructed time of flight and measured one for identified tracks using lepton ID (September 2003 data), for TOF (left) and TOFINO (right) systems.

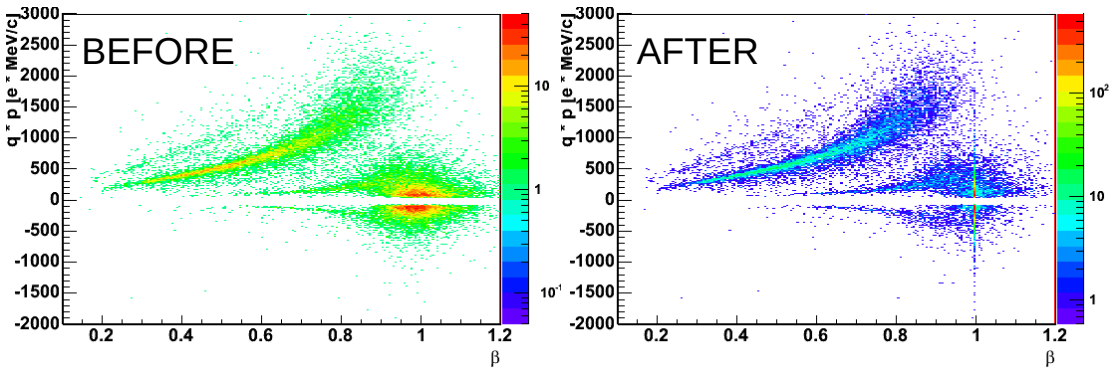

Figure 6.30 – Momentum times polarity versus β spectra before (left) and after (right) start time reconstruction, by identifying an electron/positron (September 2003 data).

By looking at Figure 6.29 the resolution values obtained from the gaussian fits (316 ps for TOF, 517 ps for TOFINO), and in particular for TOF detector, are larger respect to simulation values (162 ps for TOF, 489 ps for TOFINO). In order to compare the experimental values to the simulation ones, by a quadratic subtraction of hodoscope resolution we obtain 211 ps for TOF and 472 ps for TOFINO, which are closer to the expected values. The obtained values of the method efficiency (5σ cut) is 98.9 % for TOF, 98.1 % for TOFINO.

Figure 6.30 shows the momentum versus β spectra before and after the time reconstruction and, apart from the identified leptons, the shapes of proton and pion distributions and their good separation are maintained.

The same analysis can be done for identified negative pion cases.

Figure 6.31 and Figure 6.32 show the time difference distributions, respectively in function of momentum and integrated over all the tracks. Even in this case the contamination from misidentified leptons is present. If we check the resolution values we have 347 ps for TOF and 527 ps for TOFINO detectors; by subtracting the START resolution value we obtain 255 ps for TOF and 472 ps for TOFINO.

We must consider that in experimental data the momentum resolution is larger respect to simulation, and of course this effect is visible in the obtained reconstructed start time resolution.

In TOF plot the tail from misidentified electrons is lower respect to simulation, and then the experimental efficiency value is higher (90.1 % for TOF, 97.2 % for TOFINO).

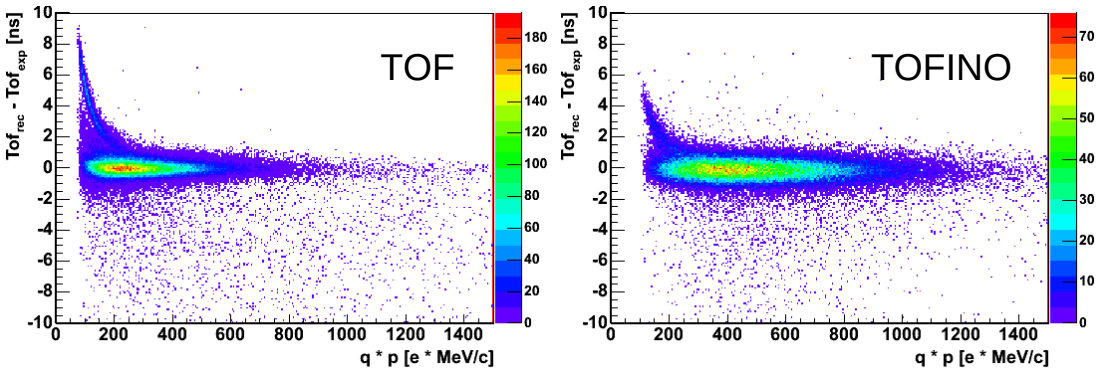

Figure 6.31 – Distributions of differences between reconstructed and measured values of tof in cases of pion identification, for September 2003 data (TOF wall on the left side, TOFINO on the right).

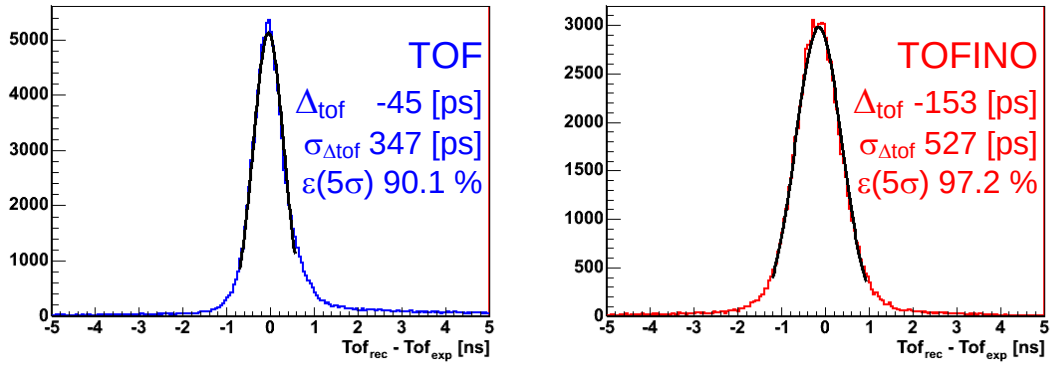

Figure 6.32 – Plots of differences between reconstructed tof and measured one of the identified negative pions (September 2003 data), for TOF (left) and TOFINO (right) systems.

In Figure 6.33 momentum versus β plots are shown before and after the start time reconstruction, and in Figure 6.34 we can see the comparison between mass distributions in the two identification cases. Even from these plots we can state the reconstruction worked properly and hadron identification is possible.

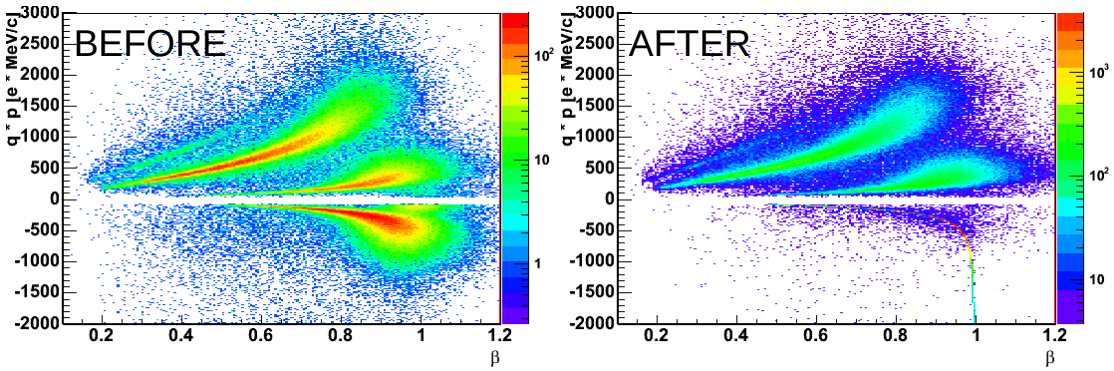

Figure 6.33 – Momentum times polarity versus β spectra before (left) and after (right) start time reconstruction, by identifying a negative pion (September 2003 data).

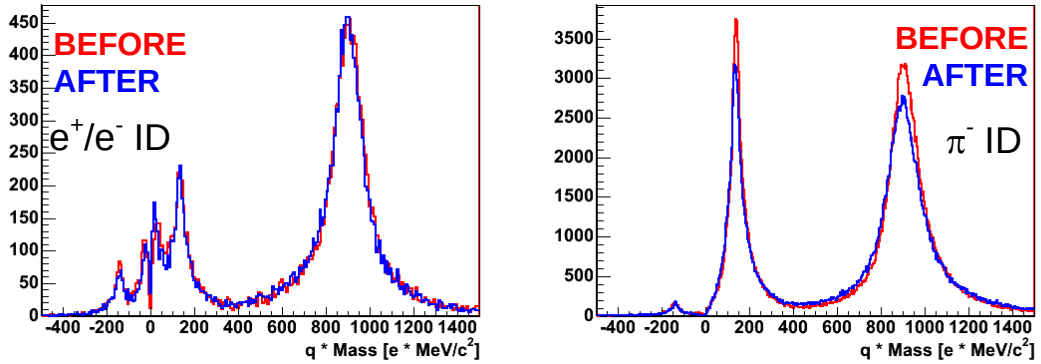

Figure 6.34 – Comparison between single particle mass distributions before and after start time reconstruction (September 2003 data).

6.5.4 January 2004 data

.

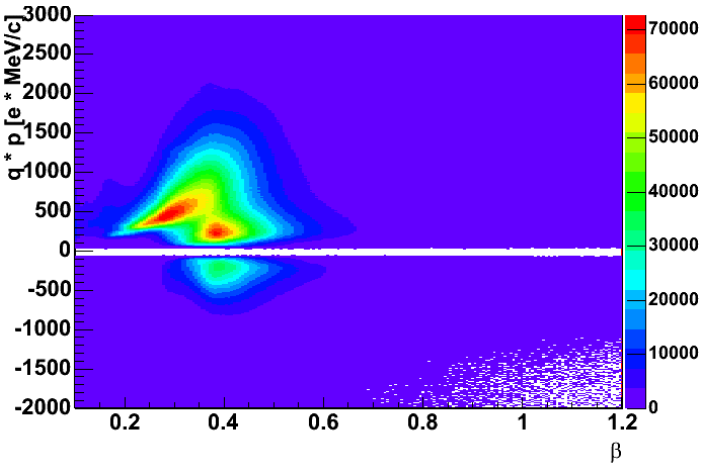

Figure 6.35 – Momentum versus β plot for January 2004 data, by taking the measured value of time of flight. In this case protons and pions are not separated and particle identification cannot be performed in this way.

During the January 2004 acquisition run the START detector was not present in the spectrometer setup, so the time measure was started from the particle which sent the first signal to 1st level trigger system. Figure 6.35 shows the momentum versus β spectrum using the time of flight values measured in this way. As expected we cannot separate in the proper way protons from pions, and it is not possible to see lepton structures as it happens with start measures.

The following pictures show the difference between the same two dimensional distributions before and after start time reconstruction, made selecting events where lepton (Figure 6.36) or pion identification (Figure 6.37) was applied.

We can see the reconstruction algorithm works quite well even when the START detector is really not present. Proton and pion distributions are well separated (the plot are in logarithmic scale) and a graphical selection is possible to identify the two kinds of particle.

At last, by checking single mass distributions (Figure 6.38) before and after the start time reconstruction, the reconstructed mass peaks are placed at the correct position

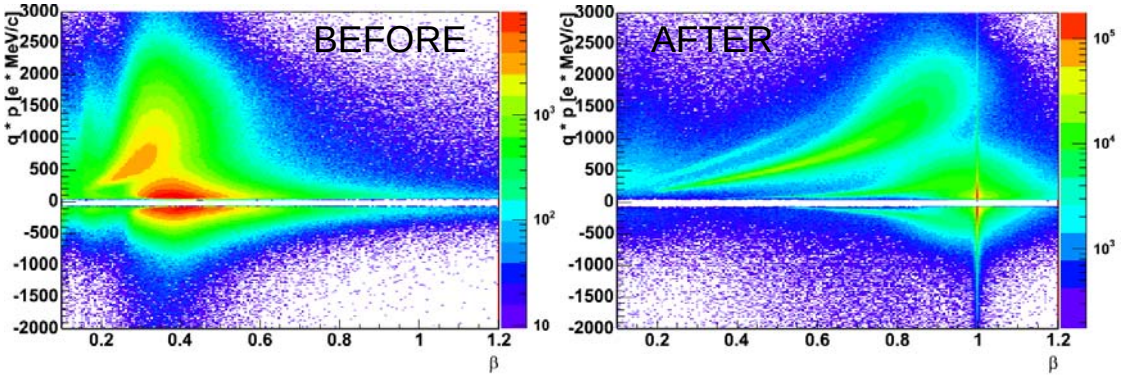

Figure 6.36 – Plots of momentum versus β for January 2004 data, before and after start time reconstruction from lepton identification.

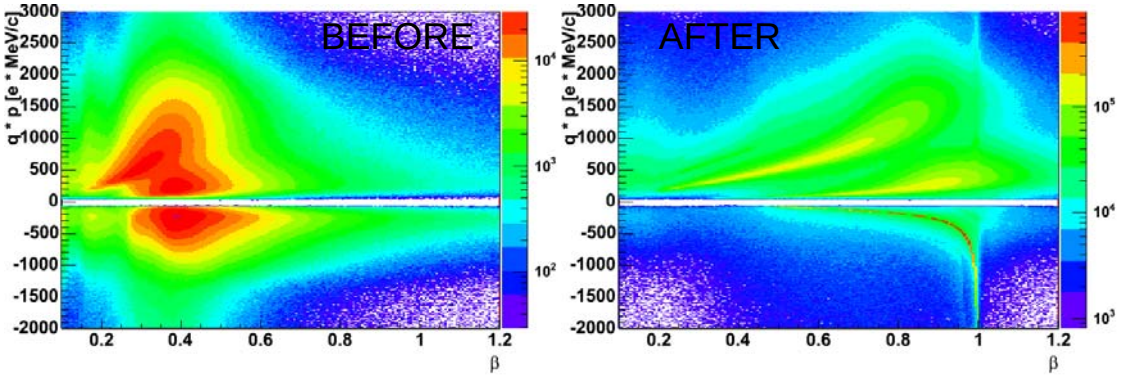

Figure 6.37 – Plots of momentum versus β for January 2004 data before and after start time reconstruction, for cases of negative pion identification.

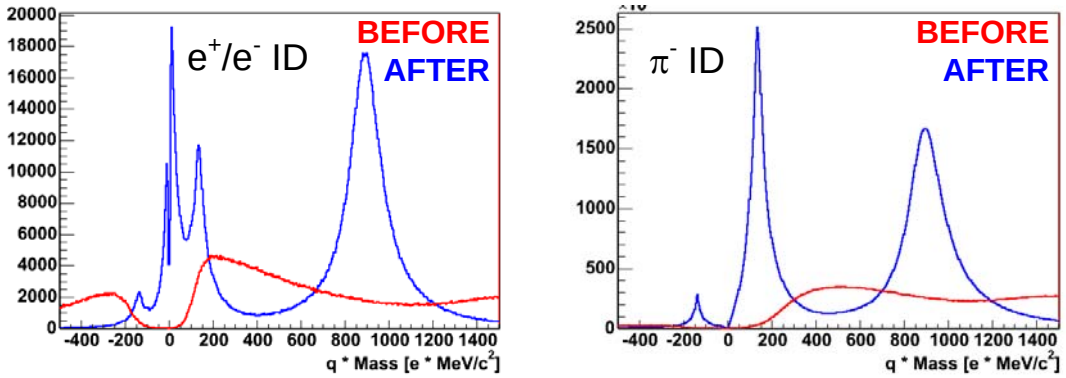

Figure 6.38 – Comparison between single particle mass distributions before and after start time reconstruction, for January 2004 data.

6.5.5 Start time reconstruction summary

In Table 6-3 all the results of start time reconstruction are presented for both simulation and September 2003 data (for January 2004 we do not have a reference time to use), in terms of time residuals between reconstructed and measured time of flight values Δtof, resolution $\sigma_{\Delta tof}$ and efficiency ε as defined in the text (number of identified tracks inside a 5 σ time window divided by the total number of identified tracks).

The absence of START detector during data acquisition make worse the time of flight measure, because of the already shown motivations. The time calibration procedure becomes much difficult and it has to use dilepton pairs (so a larger data sample respect to when START is used); the effect is visible in the worse time resolution values obtained for TOF and TOFINO detectors compared to the September 2003 data (neglecting the contribution from the START detector).

A procedure of time reconstruction was developed and tested in simulation and in experimental data acquired with the START time. His validity was demonstrated and it was applied even in January 2004 data, when the START detector was really missing. The obtained momentum versus β plots after time recalculation, which are the main tools to perform hadron particle identification for the HADES spectrometer, show a good separation between protons and pions which it was not present before.

So we can state the algorithm fulfills its goals, and it can be used to perform exclusive analysis of decay channels, where the identification of almost all the particles in the final state is required.

Data	ID	System	Δtof [ps]	$\sigma_{\Delta tof}$ [ps]	ε [%]
SIM	e^+e^-	TOF	31	162	99.8
		TOFINO	126	489	98.1
	π^+	TOF	32	192	85.1
		TOFINO	95	506	96.9
SEP03	e^+e^-	TOF	51	316	98.9
		TOFINO	-78	527	95.6
	π^+	TOF	-45	347	90.0
		TOFINO	-153	527	97.2

Table 6-3 – Summary table of results from start time reconstruction, sor simulation and September 2003 data.

NOTE

TOF position calibration: 5.3.1 per kickplane, chapter 5 per 3MDC sectors (alla fine)

TOF time calibration: equazione 6-14
The algorithm: equazione 6-25